CO_2 degassing of geothermal fluids during core-flood experiments

Chris Boeije[1*], Cas Verweij[1], Pacelli Zitha[1] and Anne Pluymakers[1]

[1] Delft University of Technology, Department of Geoscience and Engineering, Delft, The Netherlands

[*] email: c.s.boeije@tudelft.nl

Keywords: degassing, coreflood, porous media

ABSTRACT

The long-term performance of the reservoir is essential in order to ensure competitive life-cycle cost of the geothermal installations. Geothermal fluids are often saturated with gasses such as CO_2 and N_2. With their extraction from the reservoir, pressure and temperature decrease towards the extraction well. This disturbs the state of equilibrium the geothermal water is in with its dissolved components, which for gas can lead to exsolution. The exsolved gas bubbles can block the pores of the reservoir rock and therefore reduce the apparent permeability. As permeability reduction occurs mainly near the extraction well it can reduce production of geothermal waters substantially. This paper is aimed at experimentally investigating the conditions at which the onset of degassing starts and quantitively assess any associated permeability decrease. Knowledge on these parameters will enable operators to adapt their operation procedures in order to ensure long-time reservoir permeability.

This paper reports core-flood experiments where tap water containing dissolved carbon dioxide was injected into either a Bentheimer (2.3 Darcy) or Berea (140 millidarcy) sandstone core at different conditions. The first sets of core-flood experiments showed that at a temperature of 30 °C and pressure up to 50 bars the onset of the degassing process correlates closely to CO_2 solubility values obtained by the Henry's law. At these conditions CO_2 degassing near the core outlet will cause the apparent permeability to decrease by a factor 2 to 5 in the high permeability Bentheimer sandstone core. At the same conditions the apparent permeability will decrease by a factor of nearly 10 in the low permeability Berea sandstone core. The decrease in effective permeability is gradual in the Bentheimer sandstone while in the Berea sandstone the change is steeper. For rocks with small pore sizes and low absolute permeability, the reduction in effective permeability is larger and the rate of permeability decrease is faster. However, the onset of degassing is not influenced by the pore size and initial permeability. Experiments at temperatures between 30 and 90 °C show that with increasing temperature, the Van 't Hoff equation becomes less to accurate to find the degassing pressure.

1. INTRODUCTION

Geothermal waters can have various gases in solution, such as CO_2, CH_4 and N_2. During the production of these waters, a change in pressure and temperature will occur in the vicinity of the extraction well. These changes disturb the equilibrium the water is in with its dissolved gases (Pátzay et al. (1998) and can result in various problems, such as degassing (Blöcher et al. (2016). The system then goes from single-phase flow (liquid) to two-phase flow (liquid and gas). The effective pore space available for the flow of water is reduced, as part of the total pore space is taken up by gas. Therefore the effective permeability of the liquid phase will decrease (Bear 2013)

This most likely occurred at the Groß Schönebeck geothermal site in Germany, where the productivity index (PI) droppped from 8.9 m^3 /(h·MPa) to 0.6 m^3/(h·MPa), from June 2011 and November 2013. The decrease in permeability due the presence of free gas was proposed as a possible cause for the PI decline (Blöcher et al. 2016).

Despite the many observations suggesting a direct link of PI decline and release of dissolved gas, data supporting this idea and a coherent picture about the process are lacking. This study aims to address the following question:

To which extent is the flow of water in rocks limited by release of free gas from a saturated water/gas solution?

by experimentally investigating at which conditions the onset of the degassing process starts and what the effect of the degassing process on the effective water permeability. Factors influencing the degassing process and its effect on the permeability will be analyzed and discussed. These factors include the rock pore scale characteristics, temperature, and salinity.

2. MATERIALS AND METHODS

This study comprises three series of core-flood experiments in which CO_2 and an aqueous phase were co-injected into a rock core. In the first series, two rocks samples were used, having either high permeability

(Bentheimer sandstone, 2.3 D) or lower permeability (Berea sandstone, 140 mD). The temperature was set at 30 °C. The second series investigated a range of temperatures (up to 90 °C) and pressures (up to 80 bar) using only the low permeability core sample. In the third series, the effect of salinity was studied by using a higher salinity brine as the aqueous phase. This section outlines the experimental setup used in this study and the experimental procedure.

2.1 Experimental setup

Figure 1 shows a schematic of the experimental setup in these experiments. CO_2 supplied from a bottle was injected into the core using a gas booster and mass flow controller (Bronkhorst ELFLOW). The gas injection pressure was monitored using an absolute pressure transmitter (Keller PA33X, labelled p_1 in the schematic) is installed to monitor. A Quizix QX-1500 dual piston pump was used to inject the aqueous phase, here either tap water or 1M NaCl brine is used. Tap water was used instead of demineralized water to minimize the risk of the dissolution of clay particles from the cores. The rock core (40 cm long and 4 cm in diameter) is placed in a PEEK core holder, which is installed vertically in an oven that can be set to the desired temperature. Before reaching the rock core the fluids have to flow through a length of tubing in the oven (approximately 2 m in length). This allows them to reach the desired temperature and also gives the CO_2 time to mix with the water, such that only a single phase (water with dissolved CO_2) enters the core. The final length of tubing before the inlet of the core holder is transparent. This enables visual observation of the flowing fluids to ensure that the fluids are mixed properly before entering the core and no free gas bubbles are present. The fluids enter the core at the bottom, flow vertically through the core's pore space and exit at the top. A series of absolute pressure transmitters (Keller PA33X, p_2 to p_8 in the schematic.) is installed along the length of the core that allow the monitoring of the pressure at various positions during the experiment. The desired operating pressure is set using a gas-controlled back-pressure regulator (Mity Mite S-91W) installed downstream of the core.

2.2 Experimental procedure

The experiments carried out in this study are organized in several sets: each set consists of multiple experiments that aim to assess the influence of a particular variable (e.g. temperature, rock type or salinity) on the degassing process. By comparing two or more sets, the influence of these variables on the degassing process can be assessed. In each set, water and CO_2 are co-injected into the rock core.

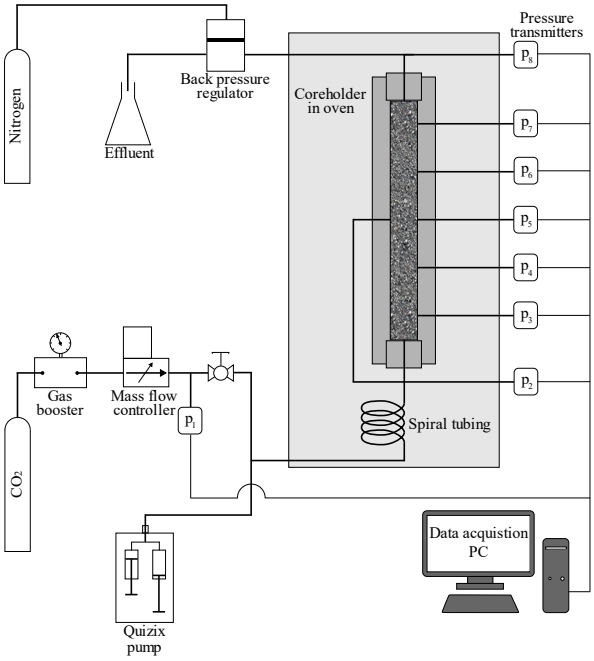

Figure 1: Schematic of experimental setup

The experiments discussed in this manuscript all use a gradually decreasing back-pressure to mimic the reducing reservoir pressure towards the production well. A similar procedure was used by (Zuo et al. 2012) in which a brine/CO_2 solution was depressurized during core-flood experiments. In each set, experiments were performed using various CO_2 concentrations. The initial back-pressure (*IBP*) was chosen sufficiently high such that the CO_2 fully dissolves in water. By lowering the back-pressure (*BP*), the point where the degassing starts, i.e. the degassing back-pressure (*DBP*), by monitoring the fluid pressure (*FP*) in the core. The formation of free gas is revealed by a significant rise of the of the *FP*.

Between each experiment the core is flushed with water to get the remaining CO_2 out. This is done by first lowering the backpressure, this causes gas expansion which forces the gas to leave the core. Then the backpressure is increased while injecting water, which results in a higher CO_2 solubility, thus causing the remaining CO_2 to dissolve in the water. Continuous flushing with water at elevated pressure allows for all of the CO_2 to be removed from the core making it ready for the next experiment. .

2.3 Data analysis

The raw data obtained from each set of experiments consists essentially of the pressures measured at each pressure transducer taken at two second intervals. The difference between two adjacent pressure transducers combined with the difference in height gives the pressure gradient over an interval. To reduce the noise in the raw data it is edited using time averaging over 20 points. This improves the signal to noise ratio of the data significantly.

The results reported in this study are mostly pressure drops over the last section of the core as a function of

the back-pressure. Since pressure is lowest in the last section degassing will start in this section. When a rapid increase of the pressure drop in the last section is observed, the *BP* measured at that point is taken as the onset of the degassing process or simply the degassing pressure (*DBP*).

The experimentally obtained *DBP* is then compared with the prediction of the bubble point from thermodynamic theory applied to the CO_2-water system. The bubble point pressure can be estimated using Henry's law (Eq [1]).

$$H_0 = \frac{s_{CO2}}{p} \qquad [1]$$

where H_0 is the value of Henry's constant at standard conditions [equal to 0.336 mol/(L·bar) for CO_2], p is the pressure in bar and s_{CO2} is the solubility of CO_2 in water at standard conditions in mol/L (Sander 2015). The solubility of gases in water typically decreases as the temperature increases. The applicability of Eq. [1] can be extended to higher temperatures by using the Van 't Hoff equation, which gives Henry's coefficient as function of the temperature $H(T)$ as:

$$H(T) = H_0 \exp\left[-\frac{\Delta_{sol}H}{R}\left(\frac{1}{T} - \frac{1}{T_0}\right)\right] \qquad [2]$$

where the term $\Delta_{sol} H$ is the enthalpy of dissolution and T_0 is the reference temperature taken here as 298.15 K. $\Delta_{sol}H/R$ is independent of temperature and, for CO_2, is equal to 2400 K (Sander 2015). The Van 't Hoff equation is used throughout this manuscript to compare the observed bubble points with the theoretical predictions. The observed pressure gradients can also be used to determine the effective core permeability by applying Darcy's law (Eq. [3]).

$$k_{eff} = \frac{Q\mu_w L}{\Delta p_m} \qquad [3]$$

where Q [m^3/s]is the volumetric flux, μ_w [Pa·s] is the water viscosity at the investigated temperature, Δp_m [Pa] is the measured pressure drop, L [m] is the length of the investigated section of the core over which the pressure drop is measured and k_{eff} [m^2]is the effective permeability of the medium based on the measured pressure drop. We have verified that for the flow rates used in this study the flow was in the laminar regime for which Darcy's law is valid.

3. RESULTS AND DISCUSSION

In this section, representative results of the experiments will be given and discussed. Since pressure is lowest towards the outlet of the core, this is the location where the first onset of degassing is expected to occur. This is why the results shown here are mostly pressure drops within this section. An overview of the conditions that were used for the various experiments is shown in Table 1.

Table 1: Overview of conditions used in the experiments

Rock type	*T* [°C]	Aqueous phase	s_{CO2} [mol/L]
Bentheimer	30	Tap water	0.85 – 1.3
Berea	30	Tap water	0.3 – 1.3
Berea	30 – 80	Tap water	0.2 – 0.4
Berea	70	1 M NaCl	0.2 – 0.8

3.1. Onset of degassing

Figure 2 displays the steady-state pressure drop as a function of back-pressure, measured over the last core section for experiments using Bentheimer rock core at 30 °C. Each line corresponds to a different CO_2 concentration. Experiments start at high back-pressure (between 40 and 50 bar for these experiments) and then the back-pressure is lowered gradually. At the highest pressures, the pressure drop remains constant, indicating single phase flow without the formation of free gas. As the back-pressure decreased, at a certain degassing back-pressure (*DBP*), an increase in the pressure drop was observed. This is indicated by opaque markers in the figure. At pressures lower than the *DBP*, the pressure drop continued to increase thus indicating a reduced ability for the water to flow.

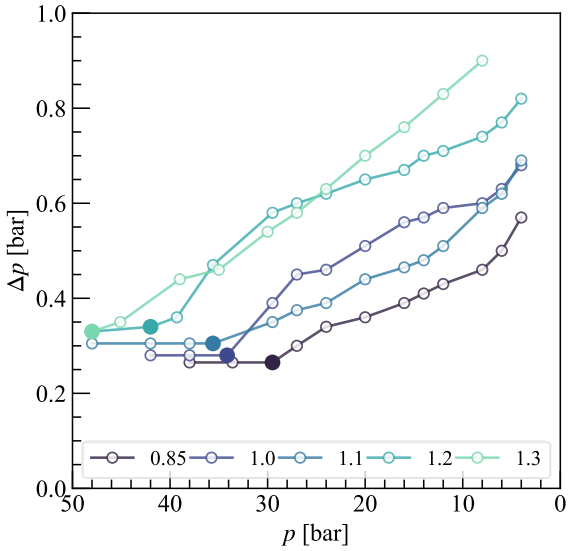

Figure 2: Pressure drop over the last interval of the core plotted against backpressure for experiments performed with different CO_2 concentrations displayed in the legend in mol/L. Opaque markers indicate the degassing back-pressure (*DBP*).

The *DBP* was compared to the theoretical solubility for CO_2 in water using Henry's law (Eq. [1]) combined with the Van 't Hoff equation (Eq. [2]) for a temperature of 30 °C. The experimentally obtained degassing points along with the theoretical prediction are given in Figure 3. Under the experimental

conditions, we expect the Van 't Hoff equation to accurately predict the degassing pressure. This is largely confirmed by the data in Figure 3.

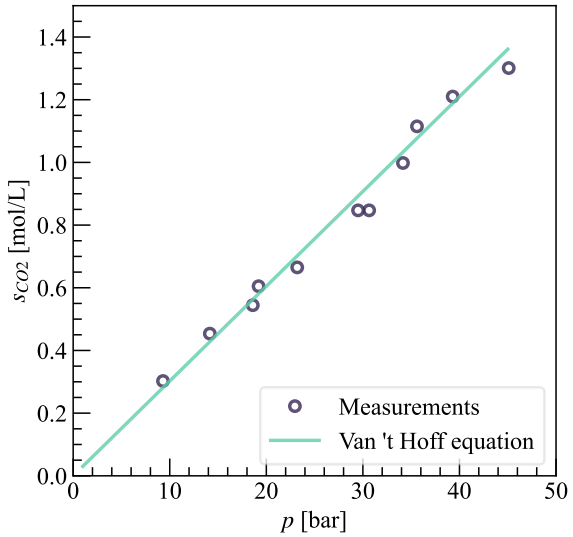

Figure 3: Measured *DBP* values for the degassing process (symbols) and their prediction using the Van 't Hoff equation (line)

Next we assess the degree to which the effective permeability of the rock is reduced due to the presence of free gas bubbles. To this end, the pressure data from Figure 2 were used to determine the effective permeability corresponding to the degassing process by applying Eq. 3. The obtained effective permeabilities are shown in Figure 4 as a function of the back-pressure. Values in this manuscript have been normalized, i.e. the ratio of the effective permeability to the absolute permeability is plotted (k_{eff} / k_{abs}) The data show a gradual decrease in effective permeability for pressures lower than *DBP*. The permeability is reduced from its original absolute value of 2.3 D to between 0.8 and 1 D thus resulting in a reduction factor of 2.3 to 3.

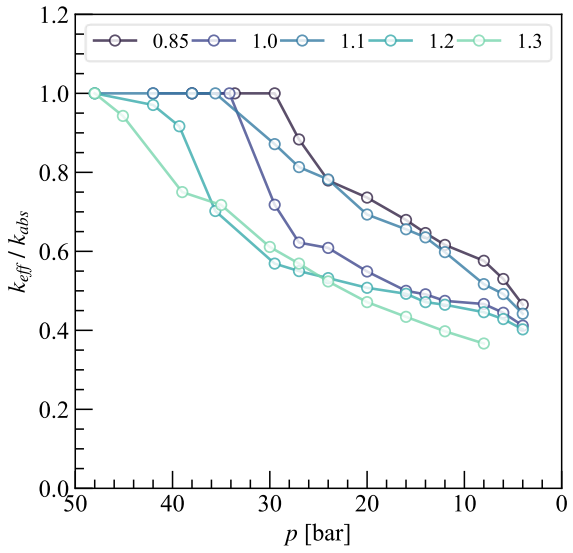

Figure 4: Effective permeability as a function of backpressure for experiments using a Bentheimer core performed with different CO_2 concentrations displayed in the legend [mol/L]

3.2. Effect of core lithology

Similar experiments were performed using a Berea rock core instead of Bentheimer to investigate the effect of lithology on the degassing process The Berea has a much lower initial permeability (0.14 D vs 2.3 D), which is caused by its smaller pores. (Al-Shakry et al. 2019) found average pore throat radii of 6 µm for the Berea vs 15 µm for Bentheimer. This has its effect on the development of the effective permeability found in this study. Figure 5 shows the effective permeability as a function of the back-pressure for the Berea experiments.

The main takeaways here are that the change between a state of single phase flow and that of blockage due to free gas formation is far more abrupt here compared to the more gradual transition found for the Bentheimer experiment. Also the extent to which the rock is blocked appears to be larger here with a decrease in effective permeability of roughly one order of magnitude (~100 → 10 mD) found for all CO_2 concentrations. This is interpreted to be a function of the kinetics of bubble growth. The Berea has more small pore throats what causes them to block earlier, because small bubbles already have the potential to block the pore throats while in the Bentheimer the small bubbles that form at the onset of the degassing process can still pass through the wider pore throats.

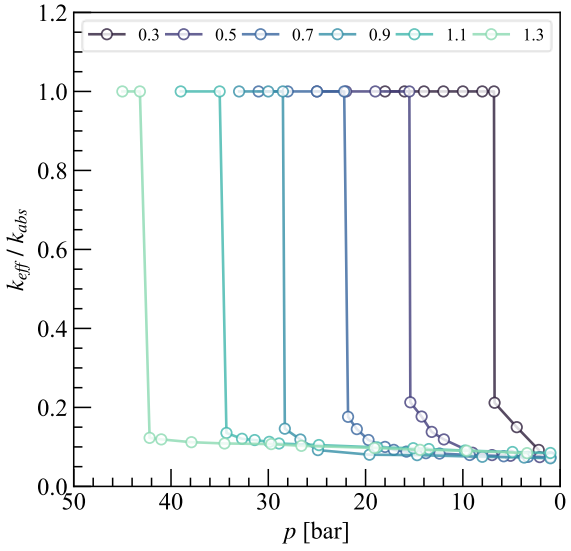

Figure 5: Effective permeability as a function of backpressure for experiments using a Berea core performed with different CO_2 concentrations displayed in the legend [mol/L]

Figure 6 shows a direct comparison of the reduction the effective permeabilities found in the Bentheimer and Berea experiments at pressures below the bubble point. This reinforces the finding in Figure 5 that the change in effective permeability happens much more abrupt for

the Berea rock than the Bentheimer. At pressures just a few bars below the onset of degassing, already a 82% reduction in permeability is found for the Berea, which rises to 91% as the pressure is reduced further. As mentioned in the introduction, (Blöcher et al. 2016) found a reduction of the productivity index of approximately 93% for the Groß Schönebeck reservoir, which is similar in magnitude as the reduction in effective permeability found here for the Berea sandstone. For the Bentheimer, the change is much more gradual and even at pressures 25 bars below the onset of degassing only a reduction of 48% is achieved.

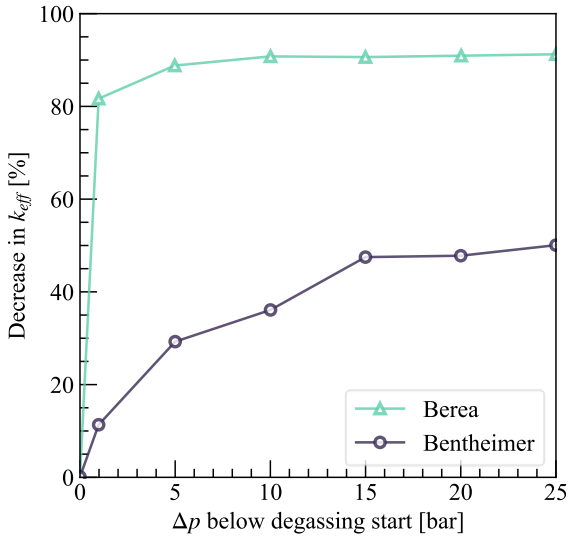

Figure 6: Comparison of the reduction in effective permeability (percentage) after the degassing process has started for the Berea and Bentheimer sandstone cores

3.3. Effect of temperature

In the second series, the influence of temperature has been investigated by repeating the experiments on Berea sandstone at a range of temperatures (30-90 °C). The resulting effective permeabilities at these temperatures for the Berea experiment are shown in Figure 7. The CO_2 concentration used here is kept at the same value of 0.4 mol/L for all investigated temperatures. Some differences in the initial permeability is found, especially for the 80 °C experiment which has a significantly higher permeability compared to the experiments at lower temperatures. A possible reason for this is that at high temperatures the PEEK core holder can become slightly ductile thereby creating a non-ideal connection between the core holder and the pressure transducer that can lead to errors in the pressure measurements. For each experiment, the effective permeability was calculated using the viscosity of water at the set temperature. Viscosity values were obtained from (Korson et al. 1969).

Higher temperatures lead to increased degassing pressures, which is to be expected due to reduced solubility. The extent to which the effective permeability is reduced is not a strong function of the temperatures, with similar values of reduction found for all investigated temperatures. For example, the 70 °C experiment showed a final reduction of 89% in permeability vs. 91% for the 30 °C experiment.

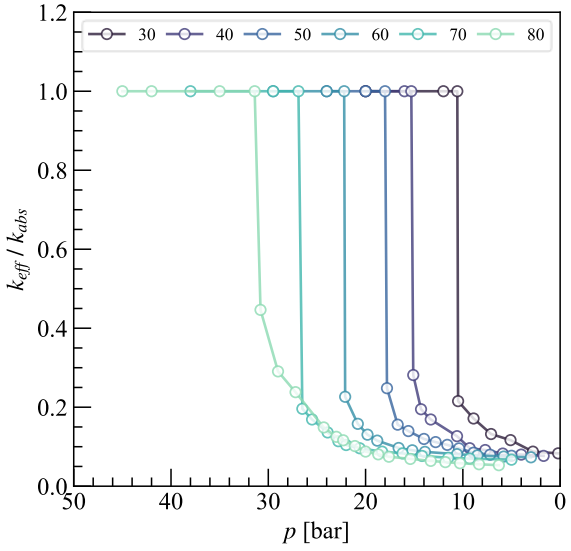

Figure 7: Comparison of the effective permeability for experiments performed at different temperatures. Legend indicates used temperature [°C]

Another set of experiments with a range of different temperatures was performed using a lower CO_2 concentration of 0.2 mol/L. The value of the degassing pressures here were lower compared to the experiments using 0.4 mol/L, but the trend that higher temperatures lead to higher degassing pressures was also found here. Both sets of experiments were also compared to the theoretical CO_2 solubility limit according to the Van 't Hoff equation. Figure 8 shows the experimentally obtained degassing pressures as a function of the temperature for both sets of experiments along with the theoretical prediction. For all temperatures, the experimentally obtained degassing pressure is lower than the theoretical prediction with higher temperatures lead to larger deviations from theory. A possible reason for this discrepancy is that the theoretical curves were created using a value of 2400 K for the enthalpy of dissolution (the term $\Delta_{sol}H/R$ in Eq. [2]). This value is up to debate and values ranging from 2200 to 2900 are found in literature (Sander 2015).

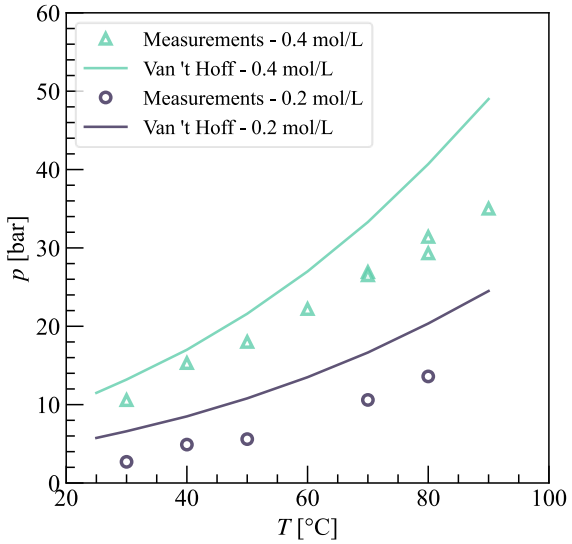

Figure 8: Onset degassing pressure as a function of temperature for experiments with a fixed CO_2 concentration of 0.2 and 0.4 mol/L along with model prediction according to the Van 't Hoff equation

3.4. Effect of brine salinity

The third series of experiments was performed to assess the influence of brine salinity on the degassing process. Here the tap water experiments are compared to experiments using a 1 M NaCl brine as the aqueous phase at 70 °C. The experiments using the NaCl brine were performed using the same CO_2 concentrations as the tap water experiments to allow for direct comparison in the degassing pressure and the extent to which the effective permeability is reduced. Figure 9 shows a comparison of the development of effective permeability for the tap water and NaCl experiments. A clear shift in degassing pressure is found between both sets of experiments. The NaCl experiments lead to degassing pressures that were between 2.5 and 3.5 bar larger than the tap water experiments. The ultimate reduction in effective permeability is very similar for both sets of experiments though indicating that the bubble nucleation and bubble growth mechanism is not affected by the increased salt concentration.

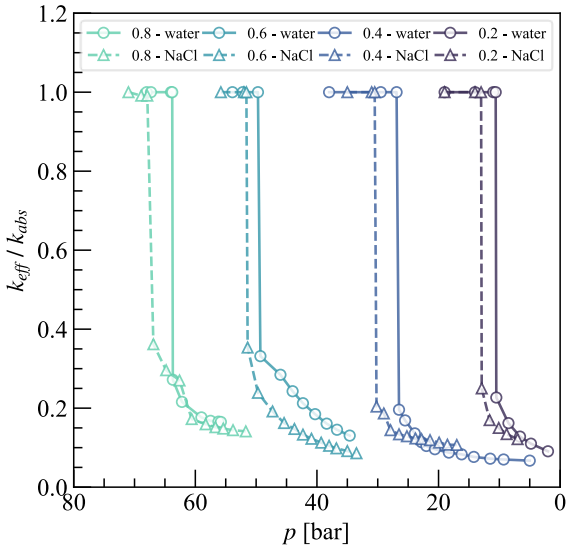

Figure 9: Comparison of effective permeability as a function of back-pressure at 70 °C for experiments using water and 1M NaCl as the aqueous phase. Legend indicates CO_2 concentration [mol/L]

The degassing onset pressures for the tap water and NaCl experiments are compared to theory in Figure 10. As was already found in Figure 8, the higher temperature experiment using tap water does not fully agree with the theoretical prediction with all degassing pressures found to occur at lower values compared to theory. In fact, the NaCl experiments show a better match with Van 't Hoff theory. The presence of salts is not included in the model though, so the observed accurate fit between the experiments and model is believed to be a coincidence.

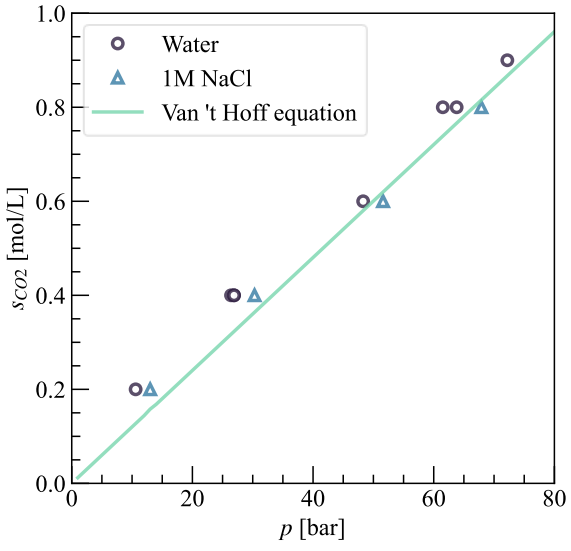

Figure 10: Onset degassing process of the water and NaCl experiments versus the Van 't Hoff equation at 70 °C

3. CONCLUSIONS

- At temperatures of 30 °C and moderate pressures (up to 50 bar), the maximum CO_2 solubility in water according to Henry's law gives a good indication for when the degassing process starts. This applicability can be extended to higher temperatures using the Van 't Hoff equation, although increased deviations from theory were found at higher temperature regimes

- The effect of the degassing process on the effective permeability of a rock is largely influenced by the pore scale characteristics of a rock. Comparing a high permeable (2.3 Darcy) Bentheimer sandstone core with a lower permeable (0.14 Darcy) Berea sandstone core shows that the degassing process causes the effective permeability to reduce faster in the low permeable Berea core than in the Bentheimer core. The total decrease in effective permeability in the Berea core is also significantly higher than in the Bentheimer core: 91% vs. 48% respectively for the experiment at 30 °C. This difference is most likely due their difference in pore throat size distribution.

- Using a 1M NaCl brine instead of tap water causes the degassing process to start at a higher pressure due to reduced CO_2 solubility. It does not change the degree to which the degassing process alters the effective permeability.

- The extent to which the effective permeability is reduced by the formation of free gas is only very slightly affected by temperature and salinity. By increasing the temperature, the total decrease in effective permeability due to degassing went from 91% to 89% at 30 and 70 °C respectively. For an increase in salinity the change in effective permeability was negligible.

REFERENCES

Al-Shakry B, Shaker Shiran B, Skauge T, Skauge A (2019) Polymer Injectivity: Influence of Permeability in the Flow of EOR Polymers in Porous Media. Paper presented at the SPE Europec featured at 81st EAGE Conference and Exhibition,

Bear J (2013) Dynamics of Fluids in Porous Media. Dover Publications, pp. 195

Blöcher G, Reinsch T, Henninges J, Milsch H, Regenspurg S, Kummerow J, Francke H, Kranz S, Saadat A, Zimmermann G, Huenges E (2016) Hydraulic history and current state of the deep geothermal reservoir Groß Schönebeck. Geothermics 63:27-43. doi:10.1016/j.geothermics.2015.07.008

Korson L, Drost-Hansen W, Millero FJ (1969) Viscosity of water at various temperatures. The Journal of Physical Chemistry 73 (1):34-39. doi:10.1021/j100721a006

Pátzay G, Stáhl G, Kármán FH, Kálmán E (1998) Modeling of scale formation and corrosion from geothermal water. Electrochimica Acta 43 (1):137-147. doi:https://doi.org/10.1016/S0013-4686(97)00242-9

Sander R (2015) Compilation of Henry's law constants (version 4.0) for water as solvent. Atmos Chem Phys 15 (8):4399-4981. doi:10.5194/acp-15-4399-2015

Zuo L, Krevor S, Falta RW, Benson SM (2012) An Experimental Study of CO2 Exsolution and Relative Permeability Measurements During CO2 Saturated Water Depressurization. Transport in Porous Media 91 (2):459-478. doi:10.1007/s11242-011-9854-2

Acknowledgements

As part of the REFLECT project, this project has received funding from the European Union's Horizon 2020 research and innovation programme under grant agreement No 850626. The authors gratefully acknowledge this support. Technical support from Michiel Slob in setting up the lab experiments at Delft University of Technology is also acknowledged.